

# MECHANISTIC MODELLING OF 9-METHYLANTHRACENE THERMOLYSIS

P.S. Virk and V.J. Vlastnik  
Department of Chemical Engineering  
M. I. T., Cambridge, MA 02139

**KEYWORDS:** Thermolysis, Mechanism, Kinetics, Numerical Simulation, Modelling.

## INTRODUCTION

**Motivation.** This work on modelling thermolysis of 9-methylanthracene, abbr 9MA, continues our studies of methylated acenes, that mimic the chemical moieties found in complex fossil materials of engineering interest. Too, since 9MA is a primary product of 9,10-dimethylanthracene, abbr 910DMA, thermolyses [1, 2], it was hoped that the present work might buttress our understanding of 910DMA thermolyses at high conversions.

**Previous Work.** Detailed mechanistic modelling of 9MA thermolysis has not hitherto been attempted. However, the literature does contain some experimental information regarding 9MA thermolysis, which we have earlier summarized [3, 4, 5, 6].

**Outline.** Our modelling of 9MA thermolysis is based upon a 19-step mechanism, valid at low conversions, that was recently formulated to describe experimental observations [3]. Thermochemical parameters for all stable and radical species occurring in the mechanism were estimated from first principles. Next, enthalpies of reaction were calculated for each elementary step and used to infer Arrhenius parameters in both forward and reverse directions. Rate constants were then calculated for each reaction at a selected temperature, and these were used in conjunction with the differential conservation relations for each species to effect a full numerical solution of the model system, starting from an initial condition of pure substrate. The numerical simulation of 9MA thermolysis kinetics and product selectivities was directly compared with experimental observations at the same conditions. A sensitivity analysis was performed to discern how errors in the estimated Arrhenius parameters affected the model results. Finally, the Arrhenius parameters of certain elementary steps were adjusted, within their error limits, to provide an optimized model that best-fit the experimental observations.

## REACTION PATHWAYS & MECHANISM

**Pathways.** Earlier experiments have identified three primary parallel pathways for thermolysis of 9MA, namely: (P1) hydrogenation to 9,10-dihydro-9-methylanthracene, abbr. DHMA, (P2) demethylation to anthracene, abbr. ANT, and (P3) methylation to 9,10-dimethylanthracene, abbr. 910DMA. The primary demethylation product ANT is associated with formation of methane gas CH<sub>4</sub>; heavy products are also formed, including both pure- and cross-termination types of dimeric species related to 9MA and DHMA, most notably a bibenzylic dimer called 9MAD.

**Mechanism.** A possible mechanism for 9MA thermolysis is presented in Fig. 1. This elementary step "graph" is constructed with substrate and all stable molecular products arrayed in the bottom row and unstable radical intermediates arrayed in the top row. Reaction "nodes", arrayed in the middle row, connect the individual species in the bottom and top rows with arrows indicating the initial direction of reaction (all reactions are, of course, reversible). Initiation reactions are denoted by solid interconnecting lines, propagation reactions by various kinds of dashed lines and termination reactions by dotted lines. Arrow weights qualitatively depict relative elementary reaction traffic, to be discussed in the next section.

The 9MA substrate is in the middle of the bottom row, with light (propagation) products to its right and heavy (termination) products to its left. The free-radical cycle is initiated by the bimolecular disproportionation of substrate (R1), an intermolecular hydrogen transfer reaction, to form the respectively dehydrogenated and hydrogenated radical species 9MA\* and HMA10\*. Of these, the latter can either abstract hydrogen from 9MA by (R2), to form DHMA product, or undergo a  $\beta$ -scission type of radical decomposition by (R3), forming ANT product and a methyl radical CH<sub>3</sub>\*. The CH<sub>3</sub>\* can either abstract H from 9MA by (R4), to form methane product, or add to 9MA by (R5), to form the dimethyl radical HDMA\*. The latter can then abstract H from 9MA via (R6) to form the observed 910DMA product. The cycle is terminated by the species 9MA\* and HMA10\* engaging in both pure- and cross-combinations, (R7-R9), to form various dimeric products. HMA10\* radical can also terminate by disproportionation, (R10), to form 9MA and DHMA. The foregoing portion of the full 9MA thermolysis mechanism is analogous to a 910DMA thermolysis mechanism devised earlier [1, 2]. However, the 9MA substrate can also form the HMA9\* radical, which can engage in all the reactions shown for HMA10\* except for C-C bond scission, giving rise to steps (R11-R22) of the full mechanism. Thus substrate disproportionation by (R11) forms 9MA\* and HMA9\*, of which the latter can abstract hydrogen from 9MA by (R12), to form DHMA product. HMA9\* can also form from H-transfer reactions (R16), between HDMA\* and 9MA, and (R17), between HMA10\* and 9MA, the latter causing radical isomerization. Finally, HMA9\* can engage in a variety of termination reactions, including combinations (R18, R19, R21) that form dimeric products, and disproportionations (R20, R22) that form 9MA and DHMA.

The proposed mechanism accounts for the major products, ANT, DMAs, DHMA, CH<sub>4</sub> and heavies, observed during the initial stages of 9MA thermolysis. Each of the observed triad of primary pathways, namely, P1 hydrogenation, P2 demethylation and P3 methylation, also arise naturally as limiting cases of the elementary step graph, with P1 comprising the sets [R1, R2, R7] and [R11, R12, R7], P2 the set [R1, R3, R4, R7] and P3 the set [R1, R3, R5, R6, R7]. The stoichiometry of these sets restricts the maximum selectivity of each major product to 1/3, which is of the magnitude of the highest selectivities observed experimentally. The mechanism also offers some theoretical insights. It suggests that the relative kinetics of hydrogenation to demethylation, (P1)/(P2), are controlled by the HMA9\* and HMA10\* radicals. The HMA10\* radical propagates both hydrogenation (R2) and demethylation (R3), but HMA9\* propagates

only hydrogenation (R12), leading to the pathway ratio  $(P1)/(P2) = [(R2)+(R12)]/(R3)$ . Further, the methylation to demethylation ratio,  $(P3)/(P2)$ , is essentially governed by competition between methyl radical reactions (R4) and (R5), in which  $\text{CH}_3^*$  either abstracts H from or adds to the 9MA substrate, the latter favoured by the presence of a potent unsubstituted 10-position.

## MODELLING

**Thermochemistry.** Enthalpies of formation,  $\Delta H_f^0$ , for all chemical species participating in our 9MA thermolysis model were estimated by a "macro" group-additivity technique, using a basis set of bond strengths,  $D^0$  kcal/mol, steric corrections,  $C^0$  kcal/mol, and stable species enthalpies of formation,  $\Delta H_f^0$ , assembled from a variety of sources cited previously [2, 7]. Fig. 2 illustrates the estimation procedures. For the stable species 9MA in (a), we started with the largest, most structurally similar basis species available, namely ANT; other basis species and steric corrections, in this case 1MN, NAP and an alkene gauche interaction, were then either added or subtracted to bridge the structural differences between the starting and the desired species. The method provided both  $\Delta H_f^0$ , kcal/mol, and its rms error, kcal/mol. Calculations for a radical species, HDMA\*, are shown in Fig. 2(b).

**Arrhenius Parameters.** Table 1 summarizes Arrhenius expressions, of the form  $\log_{10} k = \log_{10} A - E^*/\Theta$ , with rate constant  $k$  (l, mol, s units), pre-exponential factor  $A$  (same units as  $k$ ), activation energy  $E^*$  (kcal/mol), and scaled temperature  $\Theta = 0.004573*(T C + 273.2)$ , that were generated for each step of the 9MA thermolysis mechanism. An elementary reaction was first classified (column 2) according to standard free-radical reaction notation and then kinetic data for that type of reaction were analyzed to ascertain its activation parameters. Of these,  $\log_{10} A = \log_{10} A_{\text{int}} + \log_{10}(\text{rpd})$  comprised an intrinsic portion,  $\log_{10} A_{\text{int}}$  (column 3) and a reaction path degeneracy, rpd (column 4). Activation energy  $E^*$  was determined by an Evans-Polanyi expression (column 5), of form  $E^* = E_0 + \alpha \cdot \Delta H_f^0$ , with  $\alpha = 0$  (combinations), 0.5 (H-abstraction and transfer) or 1 (homolysis, beta-scission). Values of the enthalpy of reaction  $\Delta H_r^0$  (column 6), derived from thermochemical estimates of the previous section, then led to  $E^*$  (column 7) and the final Arrhenius expression (column 8).

**Numerical Solution.** The model 9MA thermolysis reaction system was solved by a computer code called ACUCHEM [8]. This program numerically solves a system of differential equations that describe the temporal behavior of a spatially homogeneous, isothermal, multicomponent chemical reaction system. Integrations are performed by the method of Gear [9], appropriate for the stiff differential equations encountered in the present case. Two types of tests were performed to ensure reliable results. First, in regard to stability, it was verified that the program generated the same concentration profiles, regardless of the time step size. Second, in regard to fidelity, the concentrations of all species, both radical and stable, calculated by the numerical solution at low conversions  $X < 0.1$  were found to agree with the corresponding concentrations obtained from pseudo-steady-state algebraic solutions at similar conditions.

## RESULTS & DISCUSSION

**Original Model.** Numerical solutions of the 9MA thermolysis model were obtained at selected conditions covering the entire experimental grid,  $315 < T C < 409$  and  $0.082 < [9MA]_0 \text{ mol/l} < 2.06$ . The complete concentration histories of all radical and stable species obtained from each simulation are used in Figs. 1, 3 and 4.

**Reaction Traffic.** The arrows in Fig. 1 graphically depict the elementary reaction traffic calculated at  $T = 370$  C,  $[9MA]_0 = 0.82$  mol/l, and very low conversion  $X \sim 0$ , the thicker arrows denoting reactions with the greater net (forward - reverse) rates. The 910DMA substrate decomposes mainly, but not exclusively, by (R1) and (R11). The rates of hydrogenation (R2) and of demethylation (R3) are of comparable magnitudes, and the rate of methyl radical quenching by H-abstraction from substrate (R4) is appreciably less than that of its addition to the substrate (R5). Among termination reactions, 9MA\* combinations, (R7) and (R18), are dominant.

**Kinetics.** Fig. 3 compares substrate decay half-lives  $t^*$  calculated from the model (hollow points and dashed lines) with those observed experimentally, (solid points and lines). Fig. 3(a), a semi-logarithmic Arrhenius-type plot of  $t^*$  vs.  $1/\Theta$ , shows that, at constant  $[9MA]_0 = 0.82$  mol/l, the calculated  $t^*$  are about 2-fold higher than experimental and exhibit a lower apparent activation energy. Fig. 3(b), a log-log plot of  $t^*$  vs.  $[9MA]_0$  at constant  $T = 370$  C, shows that the calculated  $t^*$  are 2- to 8-fold higher than experimental, the more so at the lowest  $[910DMA]_0$ , with the model predicting an apparent decomposition reaction order  $\sim 1.75$ , somewhat greater than the experimentally observed order  $\sim 1.5$ .

**Product Selectivities.** Fig. 4 compares (a) the selectivity to ANT product and (b) the ratio of 910DMA/ANT products, as calculated from the model, with those observed experimentally, using semi-logarithmic Arrhenius-type coordinates of either  $S(\text{ANT})$  or  $R(910\text{DMA}/\text{ANT})$  vs.  $1/\Theta$  at constant  $[9MA]_0 = 0.82$  mol/l. In Fig. 4(a) the model is seen to predict an ANT selectivity  $S(\text{ANT})$  from 0.2 to 0.5 orders of magnitude below experimental, while in Fig. 4(b) model predictions of the major product ratio  $R(910\text{DMA}/\text{ANT})$  lie within  $\pm 0.2$  orders of magnitude of the experimental observations.

**Sensitivity Analyses.** The significance of the differences between model predictions and experimental observations was sought from sensitivity analyses at  $T = 370$  C and  $[9MA]_0 = 0.82$  mol/l, the central point of the experimental grid, by separately perturbing the kinetics of selected elementary steps. The effects of these perturbations on the predicted decay half-life  $t^*$ , ANT selectivity  $S(\text{ANT})$ , and the primary product ratio  $R(910\text{DMA}/\text{ANT})$ , are shown by the vertical dashed lines in Figs. 3 and 4. In Figs. 3(a) and (b), for example, the uncertainty in  $t^*$  was estimated by perturbing the activation energies  $E^*_1$  and  $E^*_{11}$  by  $\pm 3.4$  and  $\pm 4.0$  kcal/mol respectively (the inherent errors in  $\Delta H_{f1}^0$  and  $\Delta H_{f11}^0$ ), since the elementary reactions R1 and R11 contribute most heavily to the destruction of 9MA substrate in our model. The upper and lower ends of the vertical dashed lines in each portion of Fig. 3 represent values of  $t^*$  obtained by joint negative and positive perturbations, respectively, of  $E^*_1$  and  $E^*_{11}$ . This sensitivity analysis shows that the inherent uncertainties of  $\pm 1.1$  orders of magnitude in values of  $t^*$  calculated by the model considerably exceed the 0.1 to 0.5 order of magnitude differences between the model results and experimental

observations. That is, within its (large) error limits, the model yields half-lives in agreement with experiments. Similar sensitivity analyses provided the vertical dashed lines in each of Figs. 4(a) and (b), showing that, within its error limits, the model also yielded 9MA selectivities and TMA/9MA ratios in accord with experiment.

**Optimized Model.** The preceding comparisons between model and experimental results are noteworthy because all the kinetic parameters employed in the original model were derived from first principles and used without adjustments. However, these comparisons also revealed the empirical alterations that might permit a best-fit of experimental results for engineering purposes, termed the "optimized" model. Specifically, the best-fit of all experimental data for 9MA thermolysis at  $T = 370$  C with  $[9MA]_0 = 0.82$  mol/l arose by altering the original activation energies ( $E^*_1, E^*_2, E^*_3, E^*_{11}, E^*_{12}, E^*_{13}, E^*_{17}, E^*_{18}$ ) by respective amounts of (-0.4, +2.2, -2.2, -0.4, +2.2, -2.2, +2.0, -2.0) kcal/mol, all of these changes being well within the inherent uncertainties of these parameters, respectively, ( $\pm 3.4, \pm 3.5, \pm 3.5, \pm 2.4, \pm 4.0, \pm 4.1, \pm 4.1, \pm 3.9, \pm 3.9$ ) kcal/mol. Figs. 5 (a) and (b) compare substrate and product histories obtained from the optimized model (lines) to the experimental data (points) for 9MA, ANT, 910DMA, CH<sub>4</sub>, and DHDMA. Fig. 5(a) shows the optimized model to well predict the observed 9MA decay, with decay half-lives  $t^* = 22000$  s from the model versus 23500 s experimental. The absolute amounts of ANT and of 910DMA formed by the model are respectively about 1.5-fold lower and higher than experimental in Fig. 5(a), and the model well predicts the relatively small amounts of DHMA, and its qualitative variation with time, in Fig. 5(b). Finally, Figs. 6(a) and (b) show that the optimized model provides the correct magnitudes of the major product ratios  $R[DHMA/ANT]$  and  $R[910DMA/ANT]$  at low conversions,  $X \rightarrow 0$ ; at higher conversions the model qualitatively follows the variation of the former ratio but not the latter.

**Modelling Perspective.** In regard to both thermolysis kinetics and the selectivities of major products, the predictions of the optimized model are appreciably closer to the experimental observations than those of the original model. However, the differences between the activation parameters of the optimized and original models, of order 2 kcal/mol, are small relative to the inherent uncertainties in these parameters, of order 4 kcal/mol. Thus, although the optimized model effects an appealing cosmetic improvement over the original model, the two models remain statistically indistinguishable. Substantive scientific improvements in modelling 9MA thermolyses must await better methods, and more reliable data, for deriving the kinetics of the underlying elementary reactions.

**ACKNOWLEDGEMENT:** This work was supported in part by Cabot Corporation, Boston, MA.

**REFERENCES**

- [1] Virk, P.S.; Vlastnik, V.J.: PREPRINTS, Div. of Petrol. Chem., ACS, **38**(2), 422 (1993).
- [2] Virk, P.S.; Vlastnik, V.J.: PREPRINTS, Div. of Fuel Chem., ACS, **39**(3), 643 (1994).
- [3] Virk, P.S.; Vlastnik, V.J.: PREPRINTS, Div. of Fuel Chem., ACS, **40**(2), 239 (1995).
- [4] Pomerantz, M.; Combs Jr., G.L.; Fink, R.: J. Org. Chem., **45**, 143 (1980).
- [5] Pope, J.M.: Ph.D. Thesis, Dept. of Chem. Eng., MIT, Cambridge, MA (1987).
- [6] Smith, C.M.; Savage, P.E.: A.I.Ch.E. J., **39**, 1355 (1993).
- [7] Vlastnik, V.J.: Sc.D. Thesis, Dept. of Chem. Eng., MIT, Cambridge, MA (1993).
- [8] Braun, W.; Herron, J.T. and Kahaner, D.K.: *Int. J. Chem. Kinet.*, **20**, 51 (1988).
- [9] Gear, C.W.: *Numerical Initial Value Problems in Ordinary Differential Equations*, Prentice-Hall, N.J., 1971.

**Table 1. Evans-Polanyi Relations and Arrhenius Parameters for Model Elementary Reactions.**

Type of Reaction	$\ln A_{ij}$ l mol <sup>-1</sup> s <sup>-1</sup>	$E_{ij}^*$ kJ	Evans-Polanyi Relation $E_{ij}^* =$	$A_{ij}$ mol <sup>-1</sup> s <sup>-1</sup>	$E_{ij}^*$ kJ/mol	Arrhenius Equation $\ln A_{ij} =$	Type of Reaction	$\ln A_{ij}$ l mol <sup>-1</sup> s <sup>-1</sup>	$E_{ij}^*$ kJ	Evans-Polanyi Relation $E_{ij}^* =$	$A_{ij}$ mol <sup>-1</sup> s <sup>-1</sup>	$E_{ij}^*$ kJ/mol	Arrhenius Equation $\ln A_{ij} =$
R1 radical depropagation	8.3	4	$AB_1^*$	43.7	43.7	$8.3 - 0.170$	R11 radical depropagation	8.3	6	$AB_1^*$	43.5	43.5	$8.3 - 0.160$
R4 radical depropagation	8.3	1	0	-43.7	0	0	B-11 radical depropagation	9.3	1	0	-43.5	0	0
R2 B-branching	8.1	3	$17.5 + AB_2^*/3$	43	17.6	$6.4 - 17.6/3$	R12 B-branching	8.1	3	$17.5 + AB_2^*/3$	1.8	18.0	$6.6 - 18.0/3$
R3 B-branching	8.1	2	$17.5 + AB_2^*/3$	43	17.6	$6.4 - 17.6/3$	R13 B-branching	8.1	1	$17.5 + AB_2^*/3$	-4.6	17.0	$6.3 - 17.0/3$
R5 methyl addition	13.3	1	$3.1 + AB_3^*$	39.3	32.3	$13.3 - 7.3/3$	R14 methyl H transfer	8.1	1	$17.5 + AB_2^*/3$	-6.0	11.0	$8.1 - 11.0/3$
R6 CH <sub>3</sub> addition	8.3	2	3.1	-39.3	3.1	$6.4 - 2.1/3$	R16 methyl H transfer	8.1	3	$17.5 + AB_2^*/3$	0.9	11.0	$8.4 - 11.0/3$
R8 B-branching	8.1	3	$17.5 + AB_2^*/3$	43.7	43	$6.4 - 13.9/3$	R17 methyl H transfer	4.3	1	$17.5 + AB_2^*/3$	-1.3	16.9	$8.1 - 16.9/3$
R4 B-branching	8.1	4	$17.5 + AB_2^*/3$	39.3	39.9	$8.7 - 20.9/3$	R17 methyl H transfer	8.1	3	$17.5 + AB_2^*/3$	1.3	18.1	$8.4 - 18.1/3$
R2 CH <sub>3</sub> addition	8.3	1	3.1	-39.3	3.1	$6.3 - 2.1/3$	R18 radical combination	9.3	1	0	-43.8	0	0
R5 methyl addition	13.3	1	$3.1 + AB_3^*$	39.3	32.4	$13.3 - 7.3/3$	R19 isomerization	13.3	1	$AB_1^*$	32.8	32.8	$13.3 - 13.3/3$
R6 methyl H transfer	8.1	1	$17.5 + AB_2^*/3$	9.3	17.0	$8.1 - 17.0/3$	R20 isomerization	13.3	1	$AB_1^*$	33.9	33.9	$13.3 - 13.3/3$
R4 methyl H transfer	8.1	1	$17.5 + AB_2^*/3$	43	17.0	$8.3 - 17.4/3$	R21 radical combination	9.3	1	0	-43.9	0	0
R7 radical combination	8.1	1	0	-43.7	0	0	R22 isomerization	13.3	1	$AB_1^*$	33.9	33.9	$13.3 - 13.3/3$
R8 radical combination	13.3	1	$AB_3^*$	34.7	34.7	$13.3 - 34.7/3$	R23 radical combination	9.3	1	0	-43.9	0	0
R9 radical combination	9.3	1	0	-43.4	0	0	R24 radical combination	9.3	1	0	-43.9	0	0
R10 isomerization	13.3	1	$AB_3^*$	32.6	32.6	$13.3 - 32.6/3$	R25 radical combination	9.3	1	0	-43.9	0	0
R11 radical combination	9.3	1	0	-43.1	0	0	R26 radical combination	9.3	1	0	-43.9	0	0
R12 isomerization	13.3	1	$AB_3^*$	32.1	32.1	$13.3 - 32.1/3$	R27 radical combination	9.3	1	0	-43.7	0	0
R13 radical depropagation	8.3	1	0	-43.9	0	0	R28 radical depropagation	8.3	3	$AB_1^*$	43.7	43.7	$8.3 - 0.170$

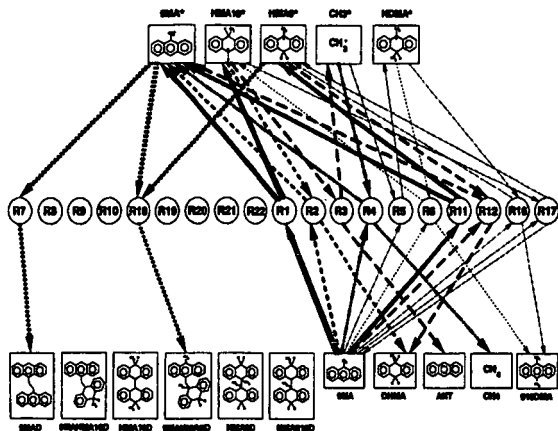


Figure 1. Elementary Step Graph of 9MA Thermolysis Mechanism. Arrow weights depict relative reaction traffic at  $T = 370\text{ C}$ ,  $[9MA]_0 = 0.82\text{ mol/l}$ , and low conversion  $X \sim 0$ , as calculated from the original model (see text).

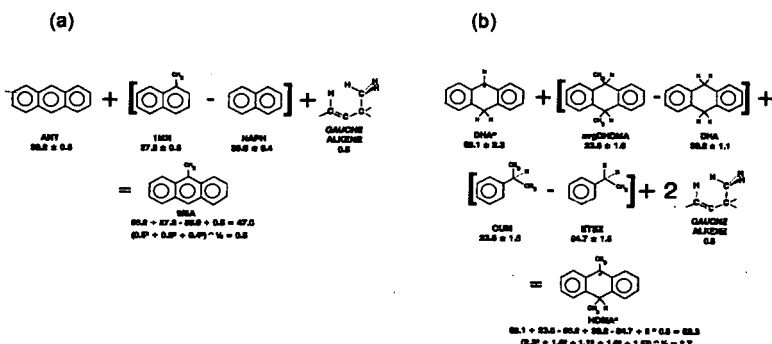


Figure 2. Illustration of Macro-Group Additivity Scheme for Estimation of Thermochemical Properties of (a) Stable and (b) Radical Species.

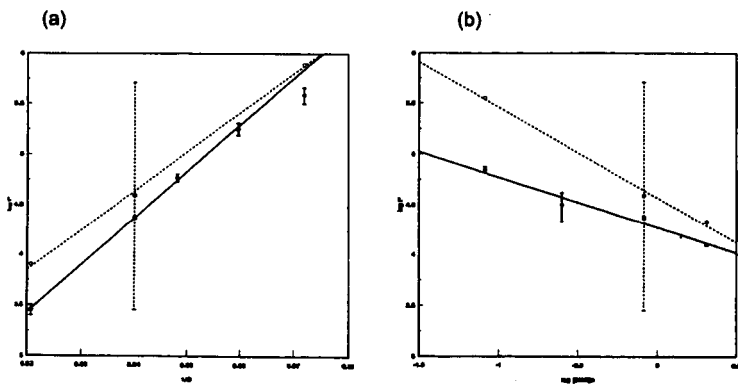


Figure 3. Decay Half-Lives  $t^*$  Experimental (solid circles and lines) Versus Calculated From Original Model (hollow circles, dashed lines) at (a) constant  $[9MA]_0 = 0.82\text{ mol/l}$  and (b) constant  $T = 370\text{ C}$ .

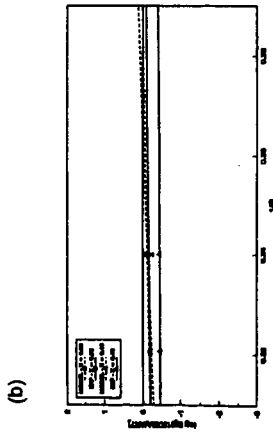
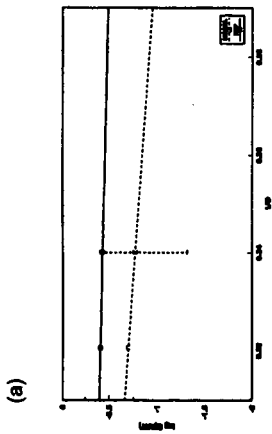


Figure 4. Original Model Results (hollow points, dashed lines) vs. Experiments (solid points, solid lines). (a) Selectivity to ANT, (b) Ratio [910DMA]/[ANT].

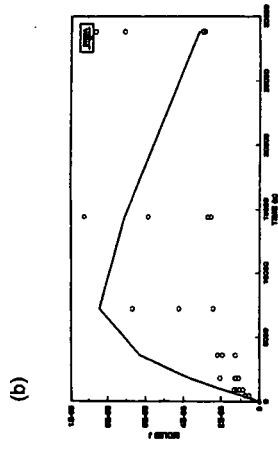
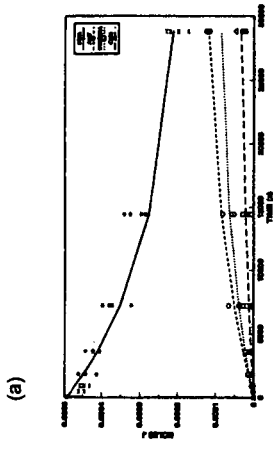


Figure 5. Optimized Model Results (lines) vs. Experiments (points) at  $T = 370\text{ C}$  with  $[9MA]_0 = 1.82\text{ mol/l}$ . (a) 9MA, ANT, CH<sub>4</sub>, 910DMA, (b) DHMA.

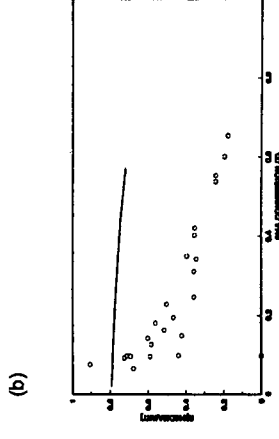
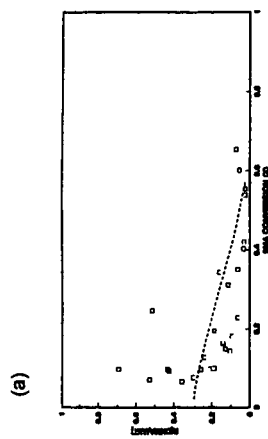


Figure 6. Optimized Model Results (lines) vs. Experiments (points) at  $T = 370\text{ C}$  with  $[9MA]_0 = 1.82\text{ mol/l}$ . (a) Ratio DHMA/ANT, (b) Ratio 910DMA/ANT.